

TransitReID: Transit OD Data Collection with Occlusion-Resistant Dynamic Passenger Re-Identification

Kaicong Huang, Talha Azfar, Jack Reilly, Ruimin Ke, *Member, IEEE*

Abstract—Transit Origin-Destination (OD) data are essential for transit planning, particularly in route optimization and demand-responsive paratransit systems. Traditional methods, such as manual surveys, are costly and inefficient, while Bluetooth and WiFi-based approaches require passengers to carry specific devices, limiting data coverage. On the other hand, most transit vehicles are equipped with onboard cameras for surveillance, offering an opportunity to repurpose them for edge-based OD data collection through visual person re-identification (ReID). However, such approaches face significant challenges, including severe occlusion and viewpoint variations in transit environments, which greatly reduce matching accuracy and hinder their adoption. Moreover, designing effective algorithms that can operate efficiently on edge devices remains an open challenge. To address these challenges, we propose TransitReID, a novel framework for individual-level transit OD data collection. TransitReID consists of two key components: (1) An occlusion-robust ReID algorithm featuring a variational autoencoder guided region-attention mechanism that adaptively focuses on visible body regions through reconstruction loss-optimized weight allocation; and (2) a Hierarchical Storage and Dynamic Matching (HSDM) mechanism specifically designed for efficient and robust transit OD matching which balances storage, speed, and accuracy. Additionally, a multi-threaded design supports near real-time operation on edge devices, which also ensuring privacy protection. We also introduce a ReID dataset tailored for complex bus environments to address the lack of relevant training data. Experimental results demonstrate that TransitReID achieves state-of-the-art performance in ReID tasks, with an accuracy of approximately 90% in bus route simulations.

Index Terms—Person Re-identification, Origin-Destination Collection, Computer Vision, Intelligent Transportation

I. INTRODUCTION

TRANSIT Origin-Destination (OD) data collection plays a critical role in the fields of transportation engineering for urban planning, service frequency adjustments, and route optimization. It aids in the analysis of relationships and impacts among regional economic development, infrastructure, and urban mobility [1]. This data represents the demand of passengers and is needed to design the bus routes efficiently to minimize travel time, reduce operating costs, and driver scheduling. As shown in Fig. 1, traditional methods for estimating transit OD data rely on manual approaches such as surveys, which are labor-intensive and suffer from low response rates [2].

More advanced methods, such as those utilizing mobile phone data [3] and Bluetooth technology [4], require passengers to carry specific devices with WiFi or Bluetooth enabled, which limits coverage and might raise privacy concerns due to the unique identifiers of the device. Automated Passenger Counters (APCs) [5] also assist in estimating OD data, however, they can only capture the aggregate number and

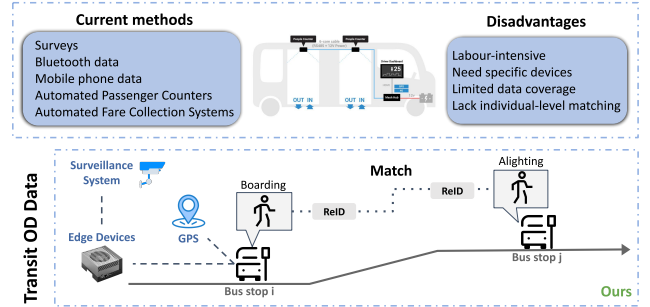


Fig. 1. Traditional methods for estimating transit OD data and our method.

locations of boarding and alighting passengers. They fail to match passengers at the individual level, which is crucial for studies focused on individual passenger behavior.

Meanwhile, most transit vehicles in the US are already equipped with onboard cameras for liability and surveillance purposes, presenting a valuable opportunity to repurpose them as smart sensors for transit OD data collection. By integrating these cameras with person re-identification (ReID) techniques and edge computing devices, seamless individual-level matching can be achieved [6]. By integrating sensors such as GPS, the matching results can be readily translated into transit OD data.

Despite the advantages of camera-based methods over prevailing techniques, their adoption in transit OD data collection remains limited due to challenges posed by the transit vehicle environment, particularly occlusion issues. For example, during peak times, boarding and alighting passengers may obscure each other from the camera view, leading to information loss and background confusion. Recent research increasingly focuses on occlusion issues in ReID, broadly categorized into two types: methods based on local attention mechanisms and those based on feature recovery. The former constructs attention mechanisms by focusing on different local areas to suppress interference from occluded parts [7], while the latter attempts to recover information from occluded areas by associating temporal or spatial information [8], [9]. Fixed local regions are used to differentiate various body parts of pedestrians and assign scores to different areas using a quality predictor in [10]. However, this fixed-area approach is not suitable for passenger matching tasks on transit vehicles under dynamic viewpoints. As the distance and angles between passengers and cameras change over time, the regions of their body parts shift throughout the video.

Due to limitations in power consumption, memory, and computational resources, edge devices are generally incapable of executing advanced and complex analytical algorithms [11], [12]. Fast and accurate estimation of OD (origin-destination) data is essential for enabling real-time passenger flow analysis in transit systems. However, most deep learning algorithms have relatively long inference times on edge devices, leading to latency and performance degradation. Some efforts have focused on model lightweighting techniques, such as knowledge distillation and pruning, or on optimizing neural network architectures specifically for edge hardware [13]. Nevertheless, lightweight models often suffer from a trade-off in performance, with reduced accuracy to some extent.

What's more, unlike traditional ReID studies, our work focuses on the problem of transit OD data collection, hence the gallery, shown in Fig. 2, is dynamic, changing with the variations in passengers boarding and alighting at each station. Consequently, ReID evolves from a problem of matching 1 query to N options, into a dynamic 1 to N_1, N_2, \dots, N_K problem, where N_k represents the size of the gallery updated at station k . To address this, we design a hierarchical storage and dynamic matching (HSDM) method to balance the trade-offs among matching accuracy, storage pressure, and processing speed.

To jointly tackle the aforementioned issues of occlusion and the constraints of online adaptive matching, we propose TransitReID, an individual-level and robust transit OD data collection method that incorporates occlusion-resistant and dynamic passenger ReID. The overall framework is shown in Fig. 3, featuring two principal technical innovations: (1) An occlusion-robust ReID algorithm that employs a region-attention module to adaptively weight less obscured body segments with clearer viewpoints, guided by a co-trained Variational Autoencoder (VAE) grading model. The VAE's reconstruction loss directly informs attention weight allocation, emphasizing visually coherent regions. This is followed by a feature fusion strategy that preserves discriminative information through concatenated weighted averages of region embeddings. (2) A Hierarchical Storage and Dynamic Matching (HSDM) mechanism specifically designed for efficient transit OD matching, which incorporates Hot/Cold Storage and a Snatch mechanism to balance accuracy, storage, and speed. A multi-threaded design is implemented to support near real-time operation on transit vehicles equipped with edge devices, without requiring any modifications to the models or architectures. Notably, the framework processes video locally on edge devices and stores only high-level, non-identifiable features, ensuring a privacy-preserving and non-intrusive solution.

Another issue is that current video ReID datasets [14]–[17] are not specifically designed for occlusion scenarios, while most occluded person ReID datasets [18]–[21] are image-based and not suited for training tasks under transit surveillance video conditions. Additionally, person images in those datasets are captured from consistent angles, whereas in transit scenarios, the angles of passenger images captured by surveillance cameras change continuously. This variability is crucial for training a robust and generalizable model under transit bus operational scenarios. Therefore, we construct a

passenger ReID dataset collected from real bus operational settings, including footage from cameras at the front and rear doors. This dataset captures 17,636 images of 157 passengers.

In essence, the major contributions of this work are as follows:

- Onboard transit surveillance systems are combined with computer vision technology to collect transit OD data, achieving individual-level precision in the construction of the OD matrix.
- An attention-based passenger ReID algorithm is specifically designed for transit vehicles scenarios with variable occlusion and viewpoints.
- A hierarchical storage and dynamic matching (HSDM) mechanism tailored for actual transit scenarios is designed, transforming the traditional static ReID problem into a dynamic ReID challenge.
- An efficient programming approach is designed to enable real-time operation on edge devices for smart transit applications. In addition, edge-based processing inherently supports privacy protection.

II. RELATED WORK

A. Transit OD Data Collection

Transit OD data collection refers to the systematic process of gathering information about the starting points (origins) and endpoints (destinations) of individual trips within a public transportation network. The most traditional and ubiquitous methods for estimating transit OD data is by surveys [22], [23], which are labor-intensive and have limited response rates. In [24], an integrated program based on Automated Fare Collection (AFC) systems was developed that can generate OD matrices and passenger load profiles by making some assumptions about round trips. A trajectory search algorithm was proposed to process passenger smart card data to track daily travel trajectories in [25]. An optimization model was proposed in [26] to approximate network-level OD flows with big data generated from Automated Passenger Counters (APCs). RFID technology was utilized to create a Boarding-In and Boarding-Out (BIBO) system for passenger monitoring in [27].

Moreover, mobile phone data [3], Bluetooth technology [4], and multi-source approaches – such as combining GIS data with passenger IC card data to construct OD matrices, as demonstrated in [28] – have been utilized. However, these methods face challenges, including high costs, significant maintenance requirements [2], and the need for passengers to carry specific devices, which limits data coverage. Additionally, the extensive use of these systems in public transport can lead to privacy concerns [29], such as exposing details about ticket types, passenger categories, travel behaviors, and purchasing methods.

While most methods capture only the number and locations of boarding and alighting passengers, they lack the precision to individually track and match passengers, crucial for detailed behavioral studies. Video-based passenger re-identification (ReID) technology combined with transit surveillance cameras provides a potential solution to this problem. In [6], the YOLO



Fig. 2. Segmentation results after detection and tracking.

algorithm is utilized to detect passengers, generating feature vectors through a neural network and selecting matches based on vector distance, but this work ignores the passive influence of occlusion. Several works [30]–[32] address the problem by only collecting information from head images of passengers inside the bus. However, this approach overlooks the potential rich information from other regions, lacks discrimination power against similar headgear, and is not robust to changes in lighting.

Our proposed methodology not only maximizes the useful information extracted from each passenger through an attention mechanism but also enhances privacy protection by processing data locally on onboard edge devices, ensuring that only high-level features are stored.

B. Occluded Re-Identification

Occlusion is by far the major problem in the computer vision-based person ReID task. Most of the occluded person re-identification methods rely on convolutional neural networks (CNNs) [7]. These aim at body part-level feature measurement, for example, a region-based quality predictor was proposed and trained with the regional feature generation model to get the weighted feature representation in [10]. However, the regions defined in this work is fixed, thus not suitable for dynamic perspectives. A pose-guided feature alignment (PGFA) [18] utilized human pose landmarks to build an attention map, guiding the model to extract useful information from non-occluded parts. Similarly, [33]–[36] utilize posture-guided attention mechanisms to discern visible areas. These methods partition the ReID problem into two segments: initially detecting key areas, then selectively extracting regional features for matching. However, the accuracy of the posture estimation model can directly impact subsequent discrimination. Other methods include feature recovery [8], [9], [37]–[39], graph convolution [40], and multi-model methods [41], [42]. Unfortunately, these methods often struggle with generalization across diverse scenarios, such as changes in viewpoints, variations in environmental lighting, and complex occlusions among passengers in transit vehicle environments. Additionally, the lack of scenario-specific training data further limits the models’ generalizability. Moreover, they address static ReID problems, whereas the gallery in a transit vehicle operating environment is inherently dynamic. We design a hierarchical storage and dynamic matching (HSDM) mechanism specifically adapted for dynamic ReID, detailed in Section III. F.

III. METHODOLOGY

A. Problem Definition

Person ReID is a computer vision problem for matching the same person across images captured by multiple heteroge-

neous cameras. In public transportation scenarios, surveillance systems in transit vehicles play a crucial role in enhancing vehicle safety and supporting operational management. However, current systems have not yet expanded to include additional artificial intelligence applications to maximize their performance. The challenges of passenger ReID in transit vehicle scenarios include temporal and spatial variations among different cameras, such as changes in lighting and varying shooting angles. The matching process is further disrupted by occlusions between passengers and between passengers and objects.

In the following sections, we focus on the transit bus environment, which is equipped with two cameras: a front-door camera C_f and a rear-door camera C_r , which capture sequences of images over a time interval T . The image sets captured by each camera are:

$$I_f = \{i_{f,1}, i_{f,2}, \dots, i_{f,T}\}, \quad I_r = \{i_{r,1}, i_{r,2}, \dots, i_{r,T}\}.$$

Each image may contain multiple passengers. The gallery, G consists of all passenger images extracted from the raw images recorded by both cameras while onboard the bus:

$$G = G_f \cup G_r = \{g_{f,1}, g_{f,2}, \dots, g_{f,M_f}\} \cup \{g_{r,1}, g_{r,2}, \dots, g_{r,M_r}\},$$

where M_f and M_r are the number of on board passengers captured by the front and rear cameras, respectively, and $M = M_f + M_r$ is the total gallery size.

At each bus stop, the query set, Q , consists of passengers departing from either the front or rear door:

$$Q = Q_f \cup Q_r = \{q_{f,1}, q_{f,2}, \dots, q_{f,N_f}\} \cup \{q_{r,1}, q_{r,2}, \dots, q_{r,N_r}\},$$

where N_f and N_r are the number of passengers alighting from the front and rear doors, respectively, and $N = N_f + N_r$ is the total number of alighting passengers.

Each passenger p_k is mapped to a high-dimensional feature space via a function:

$$\phi : p_k \rightarrow \mathbb{R}^d,$$

where d is the feature space dimension. For each alighting passenger $q_k \in Q$, we determine the best match from the gallery G by computing the distance between $\phi(q_k)$ and $\phi(g_j)$ for all $g_j \in G$, selecting the closest match:

$$\mathbf{min} \text{ distance}(\phi(q_k), \phi(g_j)), \quad \forall g_j \in G.$$

B. Detection and Tracking

The video footage recorded by the surveillance cameras at the front and rear doors of the bus is used for the research in this work. Firstly, passengers boarding and alighting are detected with YOLO11 and integrated with NVIDIA TensorRT to speed up the processing. Similar to our previous work [43], R_{door} and R_{inside} are defined in the images to respectively

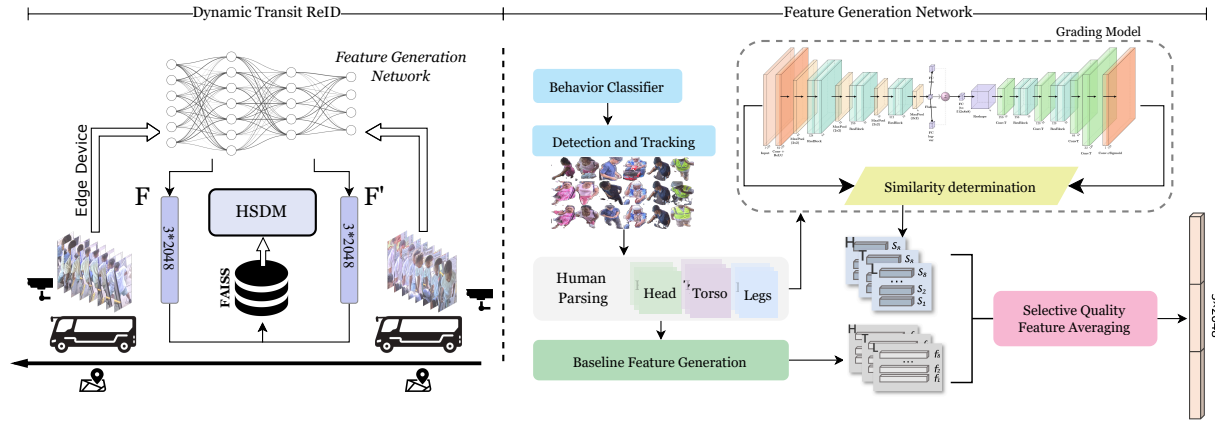


Fig. 3. The Framework of the Proposed TransitReID. In Dynamic Transit ReID, the surveillance system captures image sequences of the same passenger boarding and alighting at different stops. These images are processed by a feature generation network to extract one-dimensional feature representations. If the passenger is boarding, the features are temporarily stored in the gallery. If the passenger is alighting, the system retrieves a matching result from the gallery through the hierarchical storage and dynamic matching (HSDM) mechanism. In the Feature Generation Network, the input consists of an image sequence of a passenger. After action detection and segmentation, each mask is processed by a human parsing network, which divides the image into three body parts: ‘head’, ‘torso’, and ‘legs’. Each part is then fed into a grading model and a baseline model to obtain a quality score and an initial feature representation. Finally, a feature averaging unit integrates these outputs into the final 3*2048 length feature vector.

represent the areas outside and inside the bus door based on prior information, and the behavior of passengers is determined by the intersection and union logic of the passenger bounding box centers with the ROIs. Fig. 4 shows a case of a passenger alighting. The behavior classifier is defined with a rule-based algorithm:

Define the starting point as $S = (x_s, y_s)$ and ending point as $E = (x_e, y_e)$ for a trajectory, there are four possible conditions:

$$\begin{aligned}
 & (S \in R_{\text{inside}}) \wedge (S \notin R_{\text{door}}) \wedge (E \in R_{\text{door}}) \\
 & (S \in R_{\text{door}}) \wedge (E \in R_{\text{inside}}) \wedge (E \notin R_{\text{door}}) \\
 & (S \in R_{\text{inside}}) \wedge (S \notin R_{\text{door}}) \wedge (E \in R_{\text{inside}}) \wedge (E \notin R_{\text{door}}) \\
 & (S \in R_{\text{door}}) \wedge (E \in R_{\text{door}})
 \end{aligned} \tag{1}$$

These equations correspond to trajectories of alighting, boarding, moving while inside the bus, and moving while remaining outside. Only trajectories satisfying the first two cases are retained, with their corresponding locations recorded as key-value pairs.

It has been proven in our previous work that using segmented images can improve the accuracy of ReID, so the same processing strategy is adopted here. Fig. 2 shows some passenger images after body segmentation.

C. Data Preprocessing

Occlusion within transit vehicles significantly impacts the accuracy of conventional ReID methods, especially during peak times when multiple passengers are boarding or alighting. This can lead to information loss and background interference. The target passenger may be disturbed by non-passenger occlusions, e.g., seats or luggage, and non-target passengers [44]. Using the bounding box of the current target passenger as input can result in the loss of passenger information, such as an occluded torso, and may also introduce interference, such

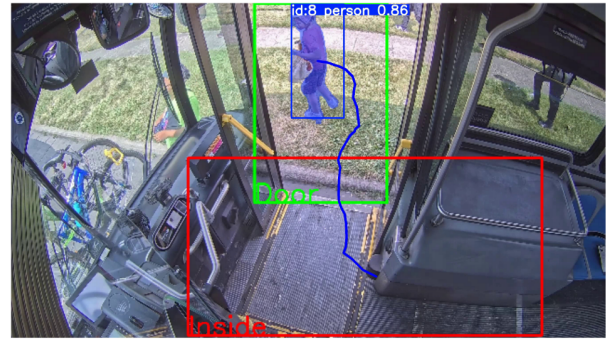


Fig. 4. One alighting example. The green box represents the outdoor area and the red box represents the area inside the bus. The blue trajectory shows the moving of the passenger.

as mistakenly including parts of other passengers’ bodies or objects, leading to feature confusion.

The segmentation algorithm mentioned in the previous section addresses the problem of background interference. To address the matching confusion caused by missing information, the global feature representation is abandoned in favor of local feature representations of different body parts. The method from [45] is employed, utilizing the Pascal-Person-Part dataset [46] which segments each passenger’s body image into 7 parts. In this work, these seven parts are aggregated into three main parts according to conventional logic: **Head**, **Torso**, and **Legs**. ‘Torso’ comprises ‘Torso’, ‘Upper Arms’, and ‘Lower Arms’, while ‘Legs’ includes ‘Upper Legs’ and ‘Lower Legs’. Each partial image is converted to gray scale image and cropped according to the minimum bounding box, then resized to 128×128 .

D. Grading Model

Passengers’ local features should be weighted differently to account for various occlusion and viewpoint scenarios.

Existing work [10] utilizes a convolutional network including a convolution layer and a fully connected layer to compute local scores. [47] designs a spatial-patch contrastive (SPC) loss to compute aggregation maps to focus on different areas. Our grading model uses a Variational Autoencoder (VAE) to assign scores to images of different body parts, where a higher score indicates better image quality, with less occlusion and a clearer viewpoint. This score will be used to calculate image weights in the subsequent processing stages.

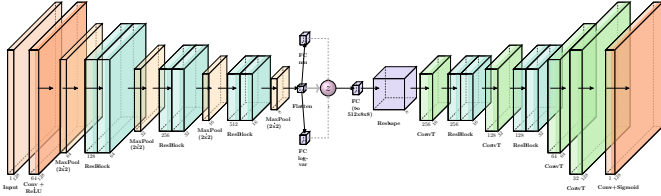


Fig. 5. Structure of the Variational Autoencoder (VAE) in the grading model.

The structure of the grading model is shown in Fig. 5. The image input passes through an encoder, which consists of a convolutional layer, followed by a max-pooling layer after each convolution. The features are then processed by residual modules to obtain a flattened feature map. Two fully connected layers calculate the mean and variance of the latent space, introducing randomness to the model and enabling better learning of reconstruction features. The decoder consists of a series of transposed convolutional layers and residual modules which output the reconstructed image through a sigmoid function.

During the training, the grading model is jointly trained with the feature extraction network Global-guided Reciprocal Learning (GRL) [48]. The underlying logic is straightforward: through training, the VAE is enabled to better reconstruct images of higher quality and poorly reconstruct those with severe occlusions and bad viewpoints. The image score, I_S , is calculated based on the joint similarity between the reconstructed and original images:

$$I_S = \sigma_1 SSIM + \sigma_2 HS + \sigma_3 MSE \quad (2)$$

To comprehensively assess the image reconstruction effect, the above formula considers three measurement factors. The Structural Similarity Index Measure (SSIM) [49] is an indicator to measure the visual similarity of two images based on three comparison parameters: luminance, contrast, and structure. Histogram Similarity (HS) focuses on the pixel value distribution of images, calculating the similarity of the histograms of the raw and reconstructed images. The Mean Squared Error (MSE) reflects the pixel value differences between the two images. The score is then fed into the Score Mapping for further process.

Score Mapping: A Logarithmic Transformation is used to map the original scores to a range from 0 to 1. Additionally, the logarithmic transformation compresses a wide score range into a smaller output range, which benefits our scenarios, where severe occlusions are of greater concern, the mapped

scores decrease rapidly, helping to effectively suppress high-occlusion situations. For cases with minor occlusions, we aim to preserve the features of these images to the greatest extent. Equation (3) defines a mapping $\mathcal{L} : x \rightarrow y$, where x is the input score and y is the transformed score. min/max is the upper/lower bound of the input. Fig. 6 displays the mapping curves at different values of k .

$$y = \frac{\log(1 + k \cdot (x - \min))}{\log(1 + k \cdot (\max - \min))} \quad (3)$$

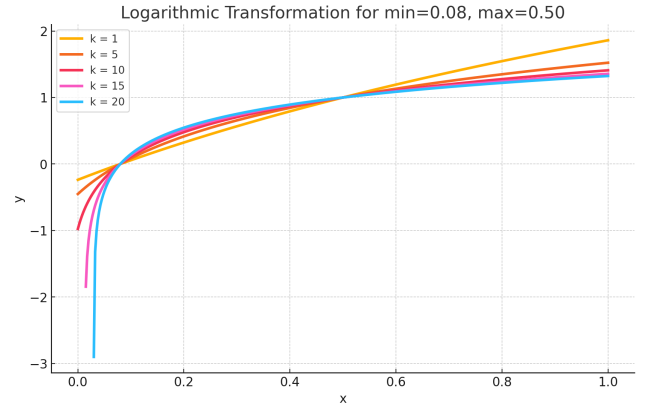


Fig. 6. Logarithmic transformation curves with different k values.

E. Selective Quality Feature Averaging

Initially, a set of images of a passenger is extracted from a video, $\{I_1, I_2, \dots, I_l\}$, where l denotes the length of the image sequence. These images are sequentially input into a feature extraction network, which outputs a fixed-length one-dimensional vector as the feature description of the passenger. We employ GRL [48] as the feature extraction network. It effectively utilizes both global and local feature correlations within video frames. This Global-guided Reciprocal Learning (GRL) framework incorporates two key modules: the Global-guided Correlation Estimation (GCE) and the Temporal Reciprocal Learning (TRL). The GCE module generates correlation maps to distinguish between high- and low-correlation features under global guidance, enhancing the model's focus on relevant features. The TRL module optimizes the use of these features over time, improving the discrimination of temporal information.

The features for three body parts Head, Torso, Legs (H, T, L), are processed separately to obtain the feature sets $\mathcal{F} = \{F_H, F_T, F_L\}$, where $F_k = \{f_1^k, f_2^k, \dots, f_l^k\}$, $k=H, T, L$. The score sets output by the grading model are denoted by $\mathcal{S} = \{S_H, S_T, S_L\}$, where $S_k = \{s_1^k, s_2^k, \dots, s_l^k\}$. We use $l = 8$ frames per person for consistency.

Unlike the baseline model [48], we do not consider all the images in a sequence. Continuing to perform weighted averaging across all images could suppress features from images containing significant information, potentially leading to confusion when identifying individuals who have similar local body features but are distinct persons. To avoid this, only

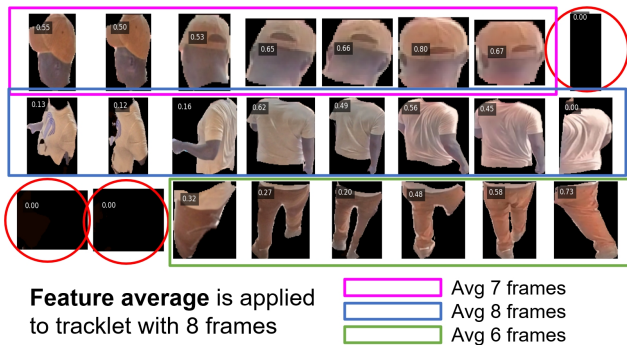


Fig. 7. Selective Quality Feature Averaging. Each image is attached with a score reflecting its degree of occlusion. Averaging all frames would suppress those of high quality. Averaging only frames with scores above a threshold, however, would preserve the features of high quality.

images with scores exceeding a certain threshold are retained, thereby preserving the contribution of high-quality images to the final feature, as depicted in Fig. 7. Ultimately, the feature vector for a passenger is calculated by the following formula:

$$\mathcal{F} = \text{CONCAT}_{k=H,T,L} \left(\frac{F_k \odot S_k}{l-d} \right) \quad (4)$$

Where d is the number of images in the sequence whose scores fall below a certain threshold. \odot is the Hadamard product. CONCAT indicates that vectors from the three parts are concatenated along the last dimension to form a one-dimensional feature vector. These features would then be stored in the Facebook AI Similarity Search (FAISS) library [50] which is an optimized library for large-scale high dimensional nearest neighbor similarity search.

F. Hierarchical Storage and Dynamic Matching

Unlike traditional ReID problems, the operational scenario in transit vehicles is dynamic and spatiotemporally continuous. This means that the passenger list onboard updates dynamically over time, resulting in a continuously changing gallery. Following normal logic, passengers in the gallery who have been matched should be removed, which not only reduces the number of samples, decreasing the error rate of subsequent matches, it also facilitates memory savings, which is crucial for edge devices with limited computing power and storage. However, since the matching accuracy is not 100%, directly deleting each match is not advisable as it could lead to error accumulation. Therefore, we propose a hierarchical storage and dynamic matching (HSDM) method to optimize the ReID problem under actual operating scenarios, with its structure shown in Fig. 8.

The HSDM consists of 3 major steps as follows, and the processing logic is summarized in Algorithm 1.

1) **Hot/Cold Matching and Storage:** The passengers are processed sequentially by bus stop in order $1 \rightarrow 2 \rightarrow \dots \rightarrow S$. The features of passengers boarding at each stop are added to the FAISS index to form a gallery. For each alighting passenger, we retrieve the Top- K candidates (in our setting $K = 5$) from FAISS, obtaining the gallery IDs from rank-1 to rank- K along with their corresponding distances. Then, the

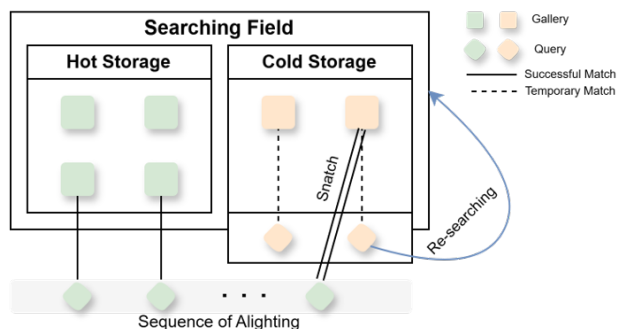


Fig. 8. Structure of hierarchical storage and dynamic matching.

match confidence γ is calculated based on the distance ratio between rank-1 and rank-2:

$$\gamma = 1 - \text{dist}_{rank1} / \text{dist}_{rank2} \quad (5)$$

A confidence threshold σ is selected based on the distribution of feature distances of positive (correct) and negative (incorrect) samples. If $\gamma > \sigma$, the match is considered successful (Hot Storage), and the matched gallery ID is deleted from FAISS. If $\gamma \leq \sigma$, it is considered a temporary match (Cold Storage), and the gallery ID is not deleted. Instead, it is recorded that the alighting passenger's temporary match is the rank-1 gallery ID, along with the remaining alternative gallery IDs (rank-2 to rank-5).

2) **Snatch:** If at the next stop or in subsequent processing, another new alighting passenger also matches a gallery ID that is still in temporary matching, and the confidence is higher, this match will snatch that gallery ID. The ID will be removed from the original alighting passenger's temporary match and matched to the snatcher, and depending on the level of confidence, it will be confirmed as a successful match (and thus removed from FAISS) or remain a temporary match. For the passenger who is snatched from, they will need to take another ID from previously stored rank-5 alternatives to attempt a match.

3) **Final Update:** After all stations have been processed, passengers who have not been matched and are still in a temporary matching state automatically transition to a successful match, and the matching accuracy for each station is then calculated.

IV. EXPERIMENTS

We evaluate the performance of this work from two aspects. First, we evaluate the passenger ReID on our own dataset and compare it with other state-of-the-art approaches. The training is on a single RTX4090 24GB GPU with the batch size, epochs, and initial learning rate set to 8, 60, and 0.0001 with a decay rate 0.1 after 30 epochs, respectively, while retaining some default settings for PFD [34] and TransReID [51]. Next, we run the simulation for transit OD data collection along a manually configured bus route on an NVIDIA Jetson AGX Orin. The confidence threshold of HSDM is set to 0.12 based on the confidence distribution of the training data. This value maximizes the discrimination between positive and

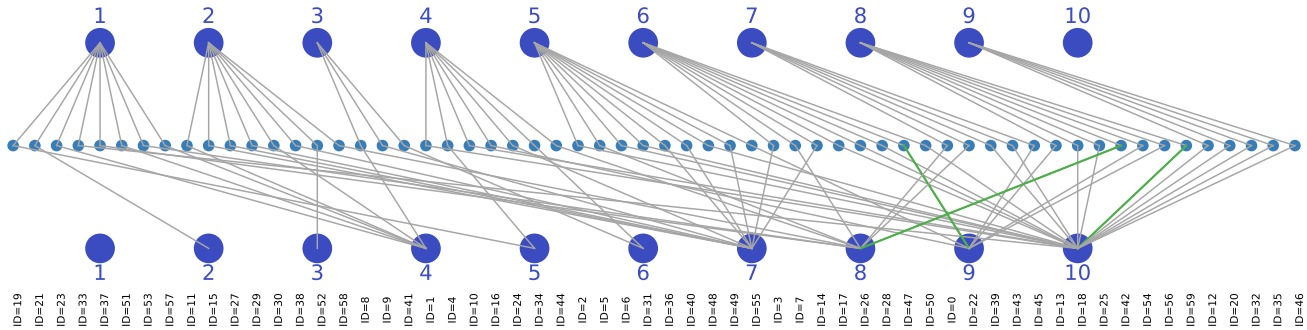


Fig. 9. OD data collection in 10 bus stops. The first and last rows represent the 10 boarding and alighting stops, while the middle row corresponds to 60 passengers. Gray lines indicate correct matches, whereas green lines represent incorrect matches.



Fig. 10. Top 5 retrieved results in the simulation with 10 bus stops. The target passengers getting off/on the bus are marked with red/green boxes. From left to right are the top 1 to 5 matched results. The IDs 13, 18, 21, 41 are correctly matched, while the IDs 42 and 47 are incorrect.

negative samples. The logarithmic transformation parameter $k = 20$. The weights $\sigma_1, \sigma_2, \sigma_3$ of the joint similarity are set to 0.2, 0.6, 0.2, respectively. To speed up processing, only 8 images are randomly sampled to form a passenger’s tracklet. The loss function follows the same setting in [48]. Performance metrics include Rank-1, 5, 10, 20, mean Average Precision (mAP), and the Cumulative Matching Characteristic (CMC) curve.

A. Bus ReID Dataset

To address the current shortage of datasets for occluded re-identification, particularly within public transportation systems, we introduce a new dataset constructed from real-time footage captured over several hours from surveillance cameras mounted at the front and rear doors of buses. The dataset contains over 17,000 images of 157 passengers, with 97 passengers in the training set and 60 in the validation set. It focuses specifically on various types and degrees of occlusions, including those between passengers and between passengers and objects. The dataset also includes images from multiple viewpoints and varying lighting conditions, posing a diverse set of challenges for model training and improving the model’s generalization capabilities in complex environments.

B. Evaluation on ReID Performance

The performance of TransitReID on traditional ReID tasks is presented in Table I, where it is compared with several state-of-the-art methods, including PGFA [18], HOREID [52], GRL [48], TransReID [51], PFD [34], and CLIP-ReID [53]. TransitReID achieves the highest accuracy among all comparative methods, improving Rank-1 accuracy by 4.7% and mAP by 8.9%. It is noteworthy that PGFA, HOREID, TransReID, and PFD are specifically designed for occluded ReID, which explains their superior performance compared to the vision-language model CLIP-ReID. Although our baseline model GRL is not specifically designed for occluded cases, it still outperforms some occluded methods due to its video-based ReID approach that learns temporal correlations. Our method not only incorporates temporal continuity information but also selectively focuses on less occluded regions from clear viewpoints to extract useful information. The experimental results show the effectiveness of our method in handling multi-view and complex occlusion scenarios specific to passenger ReID in transit environments.

Fig. 11 presents the CMC curves of TransitReID and its comparative methods from Rank-1 to Rank-20. Our method achieves nearly 100% accuracy after Rank-9. Notably, the baseline model GRL attains almost identical accuracy with ours after Rank-5, demonstrating its high performance in video-based ReID tasks. However, TransitReID significantly

Algorithm 1 HSDM: Overall Process

```

1: (Hot/Cold Matching and Storage)
2: for  $i = 1$  to  $S$  do
3:   for each passenger  $p_{\text{board}}$  boarding at station  $i$  do
4:     Add  $p_{\text{board}}$ .feature to FAISS index
5:   for each passenger  $p_{\text{alight}}$  alighting at station  $i$  do
6:      $(\text{topK\_IDs}, \text{topK\_dists}) = \text{FAISS.search}$ 
7:     Calculate  $\gamma$ 
8:     if  $\gamma > \sigma$  then
9:       Hot Storage:
10:       $p_{\text{alight}}$ .matched_ID =  $\text{topK\_IDs}[0]$ 
11:      Remove  $\text{topK\_IDs}[0]$  from FAISS index
12:     else
13:       Cold Storage:
14:       $p_{\text{alight}}$ .temp_match =  $\text{topK\_IDs}[0]$ 
15:       $p_{\text{alight}}$ .alt_IDs =  $\text{topK\_IDs}[:K]$ 
16: (Snatch)
17: for each new passenger  $p_{\text{alight2}}$  at station  $j > i$  (if exists) do
18:    $(\text{topK\_IDs2}, \text{topK\_dists2}) = \text{FAISS.search}$ 
19:   Calculate  $\gamma_2$ 
20:   if  $\text{topK\_IDs2}[0]$  is in Cold Storage by another  $p_{\text{alight}}$  then
21:     if  $\gamma_2 > \gamma_{\text{old}}$  then
22:       Remove  $\text{topK\_IDs2}[0]$  from  $p_{\text{alight}}$ .temp_match
23:     if  $\gamma_2 > \sigma$  then
24:        $p_{\text{alight2}}$ .matched_ID =  $\text{topK\_IDs2}[0]$ 
25:       Remove  $\text{topK\_IDs2}[0]$  from FAISS index
26:     else
27:        $p_{\text{alight2}}$ .temp_match =  $\text{topK\_IDs2}[0]$ 
28:        $p_{\text{alight2}}$ .alt_IDs =  $\text{topK\_IDs2}[:K]$ 
29:      $p_{\text{alight}}$  tries remaining alt_IDs and recomputes
confidence
30:   else
31:      $p_{\text{alight2}}$  tries remaining alt_IDs and recomputes
confidence
32: (Final Update)
33: for each  $p_{\text{alight}}$  still in Cold Storage and not snatched do
34:    $p_{\text{alight}}$ .matched_ID  $\leftarrow p_{\text{alight}}$ .temp_match
35: Compute final matching accuracy

```

TABLE I
COMPARISON WITH RELATED METHODS.

| Rank | Matching Rate (%) | | | | mAP |
|--------------------|-------------------|-------------|------------|------------|-------------|
| | 1 | 5 | 10 | 20 | |
| TransitReID (Ours) | 88.3 | 96.7 | 100 | 100 | 92.5 |
| PGFA [18] | 60.9 | 70.2 | 75.3 | 80.4 | 44.3 |
| HOReID [52] | 69.0 | 75.6 | 78.2 | 82.0 | 58.8 |
| GRL [48] | 75.0 | 96.7 | 100 | 100 | 83.6 |
| TransReID [51] | 83.6 | 87.1 | 89.1 | 91.4 | 78.8 |
| PFD [34] | 78.8 | 84.0 | 86.6 | 89.3 | 74.6 |
| CLIP-ReID [53] | 55.4 | 68.4 | 75.0 | 82.8 | 45.7 |

outperforms GRL from Rank-1 to Rank-4, validating its effectiveness in suppressing occlusion interference. From another perspective, it enhances the baseline model’s matching capability on ‘hard cases’, where the target gallery person often appears within the top 5 matches but fails to achieve the best match due to difficulties in extracting key features and confusion from very similar samples.

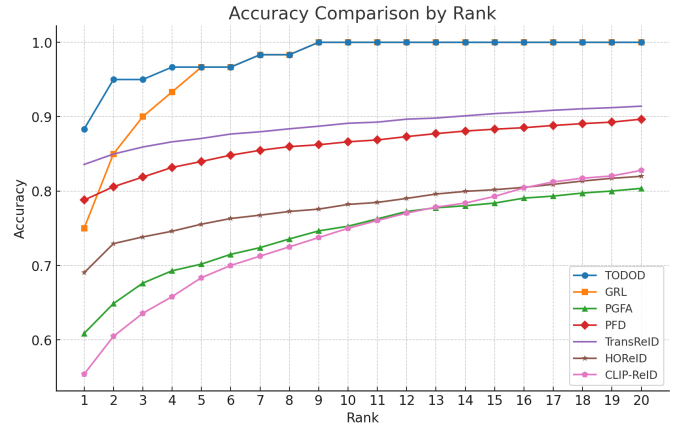


Fig. 11. Cumulative Matching Characteristic curve of different ReID methods.

Quality Information Extraction: TransitReID employs a grading model to assess images under different occlusion and viewpoint conditions. The assigned scores reflect image quality, where higher-quality images receive greater weights, contributing more information to compensate for the information loss in low-quality images. Fig. 12 visualizes the scores of four tracklet groups. Each image is divided into three segments to represent different body parts; however, this division may not precisely align with the actual body positions and is used solely for visualization purposes.

The first two rows and the last two rows correspond to eight consecutive images of two passengers, but the second and fourth rows include manually added occlusions of random size and position to better illustrate score variations. The manually occluded regions receive lower scores compared to the original images. In the third row, the passenger’s leg region receives lower scores due to a partially obstructing umbrella held in hand, whereas the exposed head and torso receive higher scores.

In the first row, from the fourth image onward, the score for the head region becomes higher than that for the body and legs, even though there is no external occlusion. This can be attributed to the increasing angle relative to the camera as the passenger fully boards the bus. This change creates a ‘folding’ effect in the image, compressing the available visual information, which can be considered a form of ‘self-occlusion’. This demonstrates that the proposed method effectively handles both external occlusions and varying viewpoints.

C. Evaluation on Dynamic Transit OD Data Collection

We randomly assign the 60 passengers in the validation set to several bus stops and randomly determine their boarding and alighting behaviors. Fig. 13 illustrates a simulation with 10 bus stops, where no passengers are on the bus before the starting stop, and passengers can only board at this stop. Similarly, at the terminal stop, all passengers on the bus are required to alight. At each stop, passengers at the stop first board the bus, followed by passengers on the bus alighting. It is worth noting that this setup may differ from real-world scenarios, where boarding and alighting occur simultaneously. As a result, the

TABLE II
PERFORMANCE ACROSS DIFFERENT NUMBERS OF BUS STOPS WITHOUT / WITH HSDM.

| Stop ID | 5 | 6 | 7 | 8 | 9 | 10 | 11 | 12 | 13 | 14 | 15 |
|---------|-------------|-------------|-------------|-------------|-------------|-------------|-------------|-------------|-------------|-------------|-------------|
| Rank-1 | 0.87 / 0.90 | 0.87 / 0.90 | 0.87 / 0.91 | 0.88 / 0.91 | 0.86 / 0.90 | 0.88 / 0.92 | 0.89 / 0.92 | 0.88 / 0.91 | 0.90 / 0.92 | 0.89 / 0.90 | 0.89 / 0.90 |
| Rank-5 | 0.96 / 0.94 | 0.95 / 0.94 | 0.95 / 0.96 | 0.95 / 0.96 | 0.95 / 0.94 | 0.95 / 0.95 | 0.95 / 0.96 | 0.95 / 0.95 | 0.95 / 0.96 | 0.95 / 0.94 | 0.95 / 0.94 |
| Rank-10 | 0.96 / 0.94 | 0.95 / 0.94 | 0.95 / 0.96 | 0.95 / 0.96 | 0.95 / 0.94 | 0.95 / 0.95 | 0.95 / 0.96 | 0.95 / 0.95 | 0.95 / 0.96 | 0.95 / 0.94 | 0.95 / 0.94 |

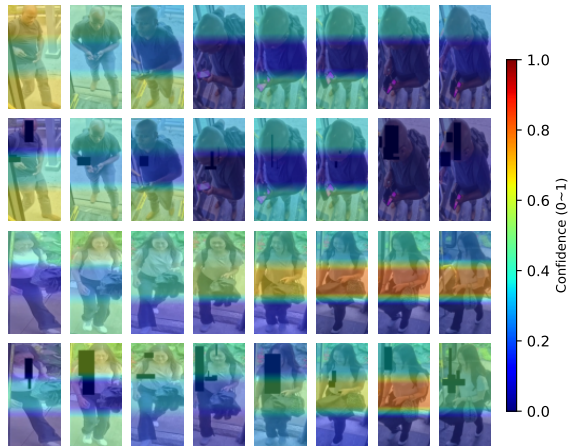


Fig. 12. Score visualization after applying the grading model. Each image is divided into three segments, corresponding to three body parts. The score is mapped to colors from dark blue to red, where a higher score indicates higher quality.

number of gallery samples at each stop in the simulation is overestimated, increasing the matching difficulty but providing a more rigorous evaluation of our method.

Fig. 9 presents the results of OD data collection. The first and last rows represent the 10 boarding and alighting stops, while the middle row represents the 60 passengers. Prediction occurs between passengers and the alighting stops, where gray lines indicate correct matches and green lines indicate incorrect matches. An incorrect match means a passenger is incorrectly matched with an alighting passenger, leading to a false prediction of the alighting stop. Out of the 60 matches, only 3 are incorrect, resulting in a total accuracy of 95%. It is important to note that this accuracy differs from the accuracy in the Ablation Study. The former represents the OD collection accuracy, while the latter represents the ReID retrieval accuracy.

Some retrieval results are shown in Fig. 10. The examples illustrate matching performance under various conditions, including different viewpoints, passenger occlusions, and both daytime and nighttime scenarios. The boarding and alighting images of the target passengers are highlighted with red and green boxes, respectively. From left to right are the top-1 to top-5 retrieval results.

The IDs 13, 18, 21, and 41 are correctly matched cases, where the top-1 retrieval result corresponds to the ground truth marked by the green box. This demonstrates the effectiveness of our method in extracting discriminative features under diverse and complex environments.

Two failure cases are also presented, corresponding to IDs 42 and 47. Specifically, ID 47 alights earlier than ID 42, and the ground truth of ID 42 is mistakenly matched as the top-1 result of ID 47. As a result, when ID 42 actually alights, its ground truth is no longer available for matching. This indicates that while the proposed HSDM strategy can reduce incorrect matches to some extent, it cannot achieve 100% accuracy. The choice of the confidence threshold for matching remains a critical factor. Nevertheless, we argue that an accuracy exceeding 90% in the simulation experiment is sufficient to validate the effectiveness of our approach in transit data collection applications.

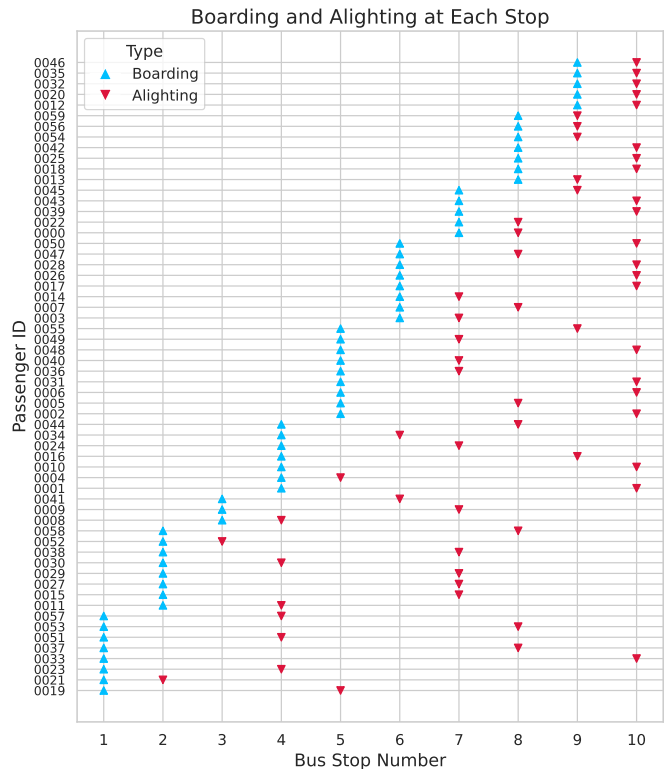


Fig. 13. Boarding and alighting simulation with 60 passengers in 10 bus stops.

D. Inference Time Analysis on Edge Devices

We conduct experiments on an NVIDIA Jetson AGX Orin to simulate the inference time of an edge computing device in a realistic transit scenario. The results are presented in Table III. Board/Alight indicates the number of passengers boarding or alighting at each stop. T_F represents the total inference time for feature extraction, and T_M represents the total time for ReID retrieval. The last row shows the average inference time

per passenger. The processing time per passenger is approximately 3 seconds, mainly constrained by the computational performance of the edge device. Nevertheless, We implement multi-threaded programming to enable real-time operation in practical smart transit applications.

As shown in Fig. 14, the video thread, connected to the transit surveillance system, captures video frames from the front and rear doors and feeds them into two separate detection threads. In these detection threads, real-time processing is achieved due to the high efficiency of the YOLO model. The featurize thread receives the detection masks, extracts feature embeddings, and handles storage, matching, and HSDM execution. The visualization thread is designed for debugging purposes and is not utilized in the practical deployment.

The real-time performance of the detection threads ensures smooth operation within the transit system. Meanwhile, the featurize thread does not require strict real-time execution—as long as the processing is completed before the next stop. For example, if 10 passengers board the bus at stop i , the entire processing should be completed within 30 seconds, before the bus arrives at stop $i + 1$.

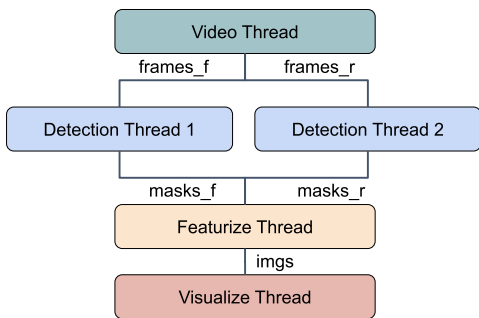


Fig. 14. Multi-threaded programming.

TABLE III
STATISTICS OF EACH STOP'S INFORMATION AND PROCESSING TIME.

| Stop ID | 1 | 2 | 3 | 4 | 5 |
|--------------|---------|---------|---------|---------|---------|
| Board/Alight | 8/0 | 8/1 | 3/1 | 7/6 | 9/2 |
| T_F | 33.4 | 30.3 | 13.2 | 42.8 | 36.0 |
| T_M | - | 1.55e-3 | 1.38e-3 | 6.30e-3 | 2.81e-3 |
| T_{mean}/P | - | 3.37 | 3.30 | 3.31 | 3.00 |
| Stop ID | 6 | 7 | 8 | 9 | 10 |
| Board/Alight | 8/2 | 5/11 | 7/9 | 5/7 | 0/21 |
| T_F | 32.7 | 52.8 | 52.0 | 39.3 | 68.2 |
| T_M | 2.72e-3 | 1.22e-2 | 1.00e-2 | 7.92e-3 | 2.14e-2 |
| T_{mean}/P | 3.27 | 3.30 | 3.06 | 2.81 | 3.25 |

E. Ablation Study

The effectiveness of the proposed HSDM mechanism is evaluated through simulations with the number of bus stops S ranging from 5 to 15. Each configuration involves 20 repeated experiments, and the average matching rate across all stops is calculated. The results are shown in Table II.

Without HSDM, the Rank-1 matching rate increases very slightly as the number of bus stops increases. This is attributed to the reduction in gallery samples at each stop, which enhances the matching success rate. With HSDM, the Rank-1 rate increases across all settings, demonstrating the mechanism's capability to handle low-confidence matches by providing these samples with additional opportunities to achieve the global optimum.

Notably, with HSDM, the Rank-1 rate remains stable regardless of the number of bus stops. This stability is achieved through the cold storage mechanism, which ensures that gallery samples at each stop are influenced not only by the number of passengers on board but also by their matching confidence. Consequently, the number of matching samples are larger than the actual number of passengers onboard, further validating the robustness of the proposed method under varying numbers of bus stops.

For Rank-5 and Rank-10, no significant changes are observed with or without HSDM, indicating the high accuracy of our ReID algorithm for simple samples.

V. CONCLUSION

This paper presented TransitReID, a novel framework for individual-level and dynamic transit OD data collection. The proposed solution addressed two critical challenges in transit environments: (1) severe occlusion through an innovative region-attention ReID mechanism that integrates a VAE-based grading model to dynamically weight visible body regions, coupled with adaptive feature fusion to preserve discriminative information; (2) continuous operation requirements via a Hierarchical Storage and Dynamic Matching (HSDM) architecture that incorporated Hot/Cold Storage and a Snatch mechanism to balance accuracy, storage, and speed. Furthermore, a multi-threaded design is implemented to achieve near real-time operation on transit vehicles equipped with edge devices. As all features are processed and stored locally, passenger privacy is effectively protected. Comprehensive evaluations demonstrated the framework's effectiveness, achieving state-of-the-art performance with 88.3% Rank-1 accuracy on our proposed transit ReID dataset and maintaining on average 90% OD estimation accuracy in real-world transit simulations.

While real video data are now available, the configuration of bus stops remains a manual process. Future work will involve deploying this system in operational public transport vehicles to conduct further tests and refinements, ensuring real-time performance. Moreover, there is a pressing need to develop lighter algorithms based on this research to facilitate real-time execution on edge devices.

VI. ACKNOWLEDGMENTS

The authors would like to express their sincere gratitude to the Urban Transportation Associates (UTA) for the valuable insights and support in this research study.

REFERENCES

- [1] Can Rong, Jingtao Ding, and Yong Li. An interdisciplinary survey on origin-destination flows modeling: Theory and techniques. *ACM Computing Surveys*, 57(1):1–49, 2024.

- [2] Vince Bernardin, Mark Bradley, Robert Chamberlin, Clint Daniels, Mark Fowler, Joel Freedman, Maren L Outwater, Kaveh Shabani, Colin Smith, William Woodford, et al. Understanding traditional origin-destination data: A survey. Technical report, United States. Federal Highway Administration, 2017.
- [3] Anahid Nabavi Larjani, Ana-Maria Olteanu-Raimond, Julien Perret, Mathieu Brédif, and Cezary Ziemlicki. Investigating the mobile phone data to estimate the origin destination flow and analysis; case study: Paris region. *Transportation Research Procedia*, 6:64–78, 2015.
- [4] Kaan Ozbay, Neveen Shlayan, Hani Nassif, et al. Real-time estimation of transit od patterns and delays using low cost-ubiquitous advanced technologies. 2017.
- [5] Yuxiong Ji, Rabi G Mishalani, and Mark R McCord. Transit passenger origin–destination flow estimation: Efficiently combining onboard survey and large automatic passenger count datasets. *Transportation Research Part C: Emerging Technologies*, 58:178–192, 2015.
- [6] Yutaka Shimada, Motoki Takagi, and Yukinobu Taniguchi. Person re-identification for estimating bus passenger flow. In *2019 IEEE Conference on Multimedia Information Processing and Retrieval (MIPR)*, pages 169–174. IEEE, 2019.
- [7] Enhao Ning, Changshuo Wang, Huang Zhang, Xin Ning, and Prayag Tiwari. Occluded person re-identification with deep learning: a survey and perspectives. *Expert systems with applications*, 239:122419, 2024.
- [8] Yuan Bian, Min Liu, Xueping Wang, Yi Tang, and Yaonan Wang. Occlusion-aware feature recover model for occluded person re-identification. *IEEE Transactions on Multimedia*, 26:5284–5295, 2024.
- [9] Zhigang Liu, Qi Wang, Miao Wang, and Yijun Zhao. Occluded person re-identification with pose estimation correction and feature reconstruction. *IEEE Access*, 11:14906–14914, 2023.
- [10] Guanglu Song, Biao Leng, Yu Liu, Congrui Hetang, and Shaofan Cai. Region-based quality estimation network for large-scale person re-identification. In *Proceedings of the AAAI conference on artificial intelligence*, volume 32, 2018.
- [11] Di Liu, Hao Kong, Xiangzhong Luo, Weichen Liu, and Ravi Subramaniam. Bringing ai to edge: From deep learning’s perspective. *Neurocomputing*, 485:297–320, 2022.
- [12] Talha Azfar, Jinlong Li, Hongkai Yu, Ruey L Cheu, Yisheng Lv, and Ruimin Ke. Deep learning-based computer vision methods for complex traffic environments perception: A review. *Data Science for Transportation*, 6(1):1, 2024.
- [13] Talha Azfar, Chengyue Wang, Ruimin Ke, Adeeba Raheem, Jeffrey Weidner, and Ruey L Cheu. Incorporating vehicle detection algorithms via edge computing on a campus digital twin model. In *International Conference on Transportation and Development 2023*, pages 400–409, 2023.
- [14] Taiqing Wang, Shaogang Gong, Xiatian Zhu, and Shengjin Wang. Person re-identification by video ranking. In *Computer Vision—ECCV 2014: 13th European Conference, Zurich, Switzerland, September 6–12, 2014, Proceedings, Part IV 13*, pages 688–703. Springer, 2014.
- [15] Liang Zheng, Zhi Bie, Yifan Sun, Jingdong Wang, Chi Su, Shengjin Wang, and Qi Tian. Mars: A video benchmark for large-scale person re-identification. In *Computer Vision—ECCV 2016: 14th European Conference, Amsterdam, The Netherlands, October 11–14, 2016, Proceedings, Part VI 14*, pages 868–884. Springer, 2016.
- [16] Yu Wu, Yutian Lin, Xuanyi Dong, Yan Yan, Wanli Ouyang, and Yi Yang. Exploit the unknown gradually: One-shot video-based person re-identification by stepwise learning. In *Proceedings of the IEEE conference on computer vision and pattern recognition*, pages 5177–5186, 2018.
- [17] Martin Hirzer, Csaba Belezna, Peter M Roth, and Horst Bischof. Person re-identification by descriptive and discriminative classification. In *Image Analysis: 17th Scandinavian Conference, SCIA 2011, Ystad, Sweden, May 2011. Proceedings 17*, pages 91–102. Springer, 2011.
- [18] Jiaxu Miao, Yu Wu, Ping Liu, Yuhang Ding, and Yi Yang. Pose-guided feature alignment for occluded person re-identification. In *Proceedings of the IEEE/CVF international conference on computer vision*, pages 542–551, 2019.
- [19] Wei-Shi Zheng, Xiang Li, Tao Xiang, Shengcai Liao, Jianhuang Lai, and Shaogang Gong. Partial person re-identification. In *Proceedings of the IEEE international conference on computer vision*, pages 4678–4686, 2015.
- [20] Lingxiao He, Jian Liang, Haiqing Li, and Zhenan Sun. Deep spatial feature reconstruction for partial person re-identification: Alignment-free approach. In *Proceedings of the IEEE conference on computer vision and pattern recognition*, pages 7073–7082, 2018.
- [21] Junyeong Kim and Chang D Yoo. Deep partial person re-identification via attention model. In *2017 IEEE International Conference on Image Processing (ICIP)*, pages 3425–3429. IEEE, 2017.
- [22] Michael R Baltes et al. Customer surveying for public transit: A design manual for on-board surveys. Technical report, National Center for Transit Research (US), 2002.
- [23] Andrew Zalewski, Daniel Sonenklar, Alexandra Cohen, Josephine D. Kressner, and Gregory S. Macfarlane. Public transit rider origin-destination survey methods and technologies. *TCRP Synthesis of Transit Practice*, 2019.
- [24] Masood Jafari Kang, Shervin Ataiean, and SM Mahdi Amiripour. A procedure for public transit od matrix generation using smart card transaction data. *Public Transport*, 13:81–100, 2021.
- [25] Daming Li, Yongjie Lin, Xinliang Zhao, Hongjun Song, and Nan Zou. Estimating a transit passenger trip origin-destination matrix using automatic fare collection system. In *Database Systems for Advanced Applications: 16th International Conference, DASFAA 2011, International Workshops: GDB, SIM3, FlashDB, SNSMW, DaMEN, DQIS, Hong Kong, China, April 22–25, 2011. Proceedings 16*, pages 502–513. Springer, 2011.
- [26] Xinyu Liu, Pascal Van Hentenryck, and Xilei Zhao. Optimization models for estimating transit network origin–destination flows with big transit data. *Journal of Big Data Analytics in Transportation*, 3(3):247–262, 2021.
- [27] Ana Belén Rodríguez González, Juan José Vinagre Díaz, and Mark Richard Wilby. Detailed origin-destination matrices of bus passengers using radio frequency identification. *IEEE Intelligent Transportation Systems Magazine*, 14(1):141–152, 2020.
- [28] Chaoqun Kong, Tangyi Guo, and Liu He. Research on od estimation of public transit passenger flow based on multi-source data. In *International Conference on Green Intelligent Transportation System and Safety*, pages 589–603. Springer, 2021.
- [29] Jinhua Zhao. *The planning and analysis implications of automated data collection systems: rail transit OD matrix inference and path choice modeling examples*. PhD thesis, Massachusetts Institute of Technology, 2004.
- [30] Junliang Guo, Yanbing Xue, Jing Cai, Zan Gao, Guangping Xu, and Hua Zhang. A bus passenger re-identification dataset and a deep learning baseline using triplet embedding. *Multimedia Tools and Applications*, 80:16425–16440, 2021.
- [31] Jiandong Zhao, Chunjie Li, Zhou Xu, Lanxin Jiao, Zhimin Zhao, and Zhibin Wang. Detection of passenger flow on and off buses based on video images and yolo algorithm. *Multimedia Tools and Applications*, 81(4):4669–4692, 2022.
- [32] Xiaoyu You, Gang Li, Yanjiao Zhao, Jie Ren, and Qiongxin Yao. Research on bus passenger flow statistics based on video images. In *2021 2nd International Conference on Electronics, Communications and Information Technology (CECIT)*, pages 937–942. IEEE, 2021.
- [33] Shang Gao, Jingya Wang, Huchuan Lu, and Zimo Liu. Pose-guided visible part matching for occluded person reid. In *Proceedings of the IEEE/CVF conference on computer vision and pattern recognition*, pages 11744–11752, 2020.
- [34] Tao Wang, Hong Liu, Pinhao Song, Tianyu Guo, and Wei Shi. Pose-guided feature disentangling for occluded person re-identification based on transformer. In *Proceedings of the AAAI conference on artificial intelligence*, volume 36, pages 2540–2549, 2022.
- [35] Zhongxing Ma, Yifan Zhao, and Jia Li. Pose-guided inter-and in-part relational transformer for occluded person re-identification. In *Proceedings of the 29th ACM international conference on multimedia*, pages 1487–1496, 2021.
- [36] Jing Xu, Rui Zhao, Feng Zhu, Huaming Wang, and Wanli Ouyang. Attention-aware compositional network for person re-identification. In *Proceedings of the IEEE conference on computer vision and pattern recognition*, pages 2119–2128, 2018.
- [37] Boqiang Xu, Lingxiao He, Jian Liang, and Zhenan Sun. Learning feature recovery transformer for occluded person re-identification. *IEEE Transactions on Image Processing*, 31:4651–4662, 2022.
- [38] Tao Wang, Mengyuan Liu, Hong Liu, Wenhao Li, Miaoju Ban, Tianyu Guo, and Yidi Li. Feature completion transformer for occluded person re-identification. *IEEE Transactions on Multimedia*, 26:8529–8542, 2024.
- [39] Mengyu Hou and Wenjun Gan. Feature pruning and recovery learning with knowledge distillation for occluded person re-identification. In *Chinese Conference on Pattern Recognition and Computer Vision (PRCV)*, pages 339–353. Springer, 2024.
- [40] Guan’an Wang, Shuo Yang, Huanyu Liu, Zhicheng Wang, Yang Yang, Shuliang Wang, Gang Yu, Erjin Zhou, and Jian Sun. High-order infor-

mation matters: Learning relation and topology for occluded person re-identification. In *Proceedings of the IEEE/CVF conference on computer vision and pattern recognition*, pages 6449–6458, 2020.

- [41] Ammarah Farooq, Muhammad Awais, Josef Kittler, and Syed Safwan Khalid. Axm-net: Implicit cross-modal feature alignment for person re-identification. In *Proceedings of the AAAI conference on artificial intelligence*, volume 36, pages 4477–4485, 2022.
- [42] Frank M Hafner, Amran Bhuyian, Julian FP Kooij, and Eric Granger. Cross-modal distillation for rgb-depth person re-identification. *Computer Vision and Image Understanding*, 216:103352, 2022.
- [43] Jiachen Ye, Talha Azfar, and Ruimin Ke. Real-time transit origin-destination data collection via edge-ai-based passenger re-identification. In *Transportation Research Board Poster Session 2025*, 2025.
- [44] Zhikang Wang, Feng Zhu, Shixiang Tang, Rui Zhao, Lihuo He, and Jiangning Song. Feature erasing and diffusion network for occluded person re-identification. In *Proceedings of the IEEE/CVF conference on computer vision and pattern recognition*, pages 4754–4763, 2022.
- [45] Peike Li, Yunqiu Xu, Yunchao Wei, and Yi Yang. Self-correction for human parsing. *IEEE Transactions on Pattern Analysis and Machine Intelligence*, 2020.
- [46] Xianjie Chen, Roozbeh Mottaghi, Xiaobai Liu, Sanja Fidler, Raquel Urtasun, and Alan Yuille. Detect what you can: Detecting and representing objects using holistic models and body parts. In *Proceedings of the IEEE conference on computer vision and pattern recognition*, pages 1971–1978, 2014.
- [47] Xiaokang Zhang, Yan Yan, Jing-Hao Xue, Yang Hua, and Hanzi Wang. Semantic-aware occlusion-robust network for occluded person re-identification. *IEEE Transactions on Circuits and Systems for Video Technology*, 31(7):2764–2778, 2020.
- [48] Xuehu Liu, Pingping Zhang, Chenyang Yu, Huchuan Lu, and Xiaoyun Yang. Watching you: Global-guided reciprocal learning for video-based person re-identification. In *Proceedings of the IEEE/CVF conference on computer vision and pattern recognition*, pages 13334–13343, 2021.
- [49] Zhou Wang, Alan C Bovik, Hamid R Sheikh, and Eero P Simoncelli. Image quality assessment: from error visibility to structural similarity. *IEEE transactions on image processing*, 13(4):600–612, 2004.
- [50] Matthijs Douze, Alexandr Guzhva, Chengqi Deng, Jeff Johnson, Gergely Szilvasy, Pierre-Emmanuel Mazaré, Maria Lomeli, Lucas Hosseini, and Hervé Jégou. The faiss library. 2024.
- [51] Shuting He, Hao Luo, Pichao Wang, Fan Wang, Hao Li, and Wei Jiang. Transreid: Transformer-based object re-identification. In *Proceedings of the IEEE/CVF International Conference on Computer Vision (ICCV)*, pages 15013–15022, October 2021.
- [52] Guan'an Wang, Shuo Yang, Huanyu Liu, Zhicheng Wang, Yang Yang, Shuliang Wang, Gang Yu, Erjin Zhou, and Jian Sun. High-order information matters: Learning relation and topology for occluded person re-identification. In *The IEEE/CVF Conference on Computer Vision and Pattern Recognition (CVPR)*, June 2020.
- [53] Siyuan Li, Li Sun, and Qingli Li. Clip-reid: exploiting vision-language model for image re-identification without concrete text labels. In *Proceedings of the AAAI Conference on Artificial Intelligence*, volume 37, pages 1405–1413, 2023.



Talha Azfar is a Ph.D. student in Transportation Engineering at Rensselaer Polytechnic Institute (RPI) since August 2023. He began his Ph.D. in the University of Texas at El Paso in 2022. His research focus lies in the intersection of computer vision, digital twins, edge computing, and intelligent transportation infrastructure. Talha holds a Masters degree in Systems Engineering from PIEAS, Islamabad (2016), and a Bachelors in Electrical Engineering from NUST, Islamabad (2014).



Jack Reilly is a Professor of Practice in the Department of Civil and Environmental Engineering at Rensselaer Polytechnic Institute in Troy, NY where he teaches courses in transportation engineering, policy and design. He has been on the RPI faculty for 15 years. Dr. Reilly is a proud RPI alumnus having received a bachelor's, master's and doctoral degree from that school. During most of his professional career, he was on the management staff of the Capital District Transportation Authority, responsible for service planning, capital project development, information technology and federal relations. Dr. Reilly was the project manager for the Rensselaer Rail Station. He has done extensive consulting work in transportation planning and operations throughout the United States, and has served as a consultant to the World Bank on Intelligent Transportation System projects in India and China.



Ruimin Ke is an Assistant Professor in the Department of Civil and Environmental Engineering at Rensselaer Polytechnic Institute. Dr. Ke possesses profound expertise in intelligent transportation systems (ITS), with a specialization in developing machine learning algorithms and advanced computing systems tailored for ITS applications. Dr. Ke's academic background includes a Ph.D. and M.S. in Transportation Engineering from the University of Washington, an M.S. in Computer Science from the University of Illinois Urbana-Champaign, and a B.E. in Automation from Tsinghua University. He holds memberships in the TRB standing committee on Artificial Intelligence and Advanced Applications (AED50), the TRB standing committee on Statewide/National Transportation Data and Information Systems (AED10), the ASCE T&DI Infrastructure Systems Committee, the ASCE T&DI Artificial Intelligence in Transportation committee, and IEEE.



Kaicong Huang is a Ph.D. student in Transportation Engineering at Rensselaer Polytechnic Institute (RPI) since August 2024. He holds a M.S. in Robotics from National University of Singapore (2024), and a B.E. in Electronic Engineering from Sun Yat-sen University (2023). His research interests include computer vision, autonomous vehicles, and intelligent transportation systems.